Flux Qubits with Long Coherence Times for Hybrid Quantum Circuits

M. Stern,[1,*] G. Catelani,[2] Y. Kubo,[1] C. Grezes,[1] A. Bienfait,[1] D. Vion,[1] D. Esteve,[1] and P. Bertet[1]
[1]*Quantronics Group, SPEC, IRAMIS, DSM, CEA Saclay, 91191 Gif-sur-Yvette, France*
[2]*Forschungszentrum Jülich, Peter Grünberg Institut (PGI-2), 52425 Jülich, Germany*
(Received 3 July 2014; published 19 September 2014)

We present measurements of superconducting flux qubits embedded in a three dimensional copper cavity. The qubits are fabricated on a sapphire substrate and are measured by coupling them inductively to an on-chip superconducting resonator located in the middle of the cavity. At their flux-insensitive point, all measured qubits reach an intrinsic energy relaxation time in the 6–20 μs range and a pure dephasing time comprised between 3 and 10 μs. This significant improvement over previous works opens the way to the coherent coupling of a flux qubit to individual spins.

DOI: 10.1103/PhysRevLett.113.123601 PACS numbers: 42.50.Pq, 85.25.Cp

Electronic spins in semiconductors such as nitrogen vacancy centers in diamond or phosphorus donors in silicon can reach coherence times up to seconds [1–3] and are therefore promising candidates for quantum information processing. However, the main obstacle to an operational spin-qubit quantum processor is the difficulty of coupling distant spins. To solve this issue, it has been proposed to couple each spin to a superconducting circuit which acts as a quantum bus and mediates the spin-spin interaction [4,5]. This approach requires reaching the strong coupling regime where the coupling strength g between the spin and the circuit is larger than their respective decoherence rates. Among all superconducting circuits, the largest coupling constants could be obtained with flux qubits (FQ) [6–13] due to their large magnetic dipole. They can reach up to $g/2\pi \sim 100$ kHz for realistic parameters, which is much larger than the best reported spin decoherence rates. This brings a strong motivation for developing FQs with a coherence time $T_2 > 2/g \sim 4$ μs.

FQ coherence times reported up to now are limited to $T_2 \lesssim 2$ μs, with a sizeable irreproducibility [10,13]. The reasons for these relatively short coherence times are numerous but stem in part from the poor control of the electromagnetic environment of the qubit in previously used dc-SQUID readout setups [9–11]. A better control of the environment was recently demonstrated in the case of another superconducting qubit, the transmon, by using a three dimensional (3D) cavity that allows reading out the qubit and protecting it from spontaneous emission [14]. A natural question is therefore whether it is also possible to increase the coherence times of FQs and their reproducibility by using such a setup.

In this work, we present the first measurements of FQs in a 3D cavity. The six qubits measured reach reproducible coherence times T_2 between 2 and 8 μs, which would be already sufficient to reach the strong-coupling regime with a single spin. In addition, our results shed light on decoherence of FQs, giving evidence that charge noise is the dominant decoherence mechanism at their flux-insensitive point.

A scheme of the three dimensional cavity used in our experiment is shown in Fig. 1(a). The cavity is made of copper to enable the application of an external magnetic field B to the FQs. Its dimensions are chosen for its first mode to be at 5.6 GHz. The sample inserted in the cavity is a sapphire chip with an LC resonator inductively coupled to six FQs, with a coupling constant ~50 MHz. The LC

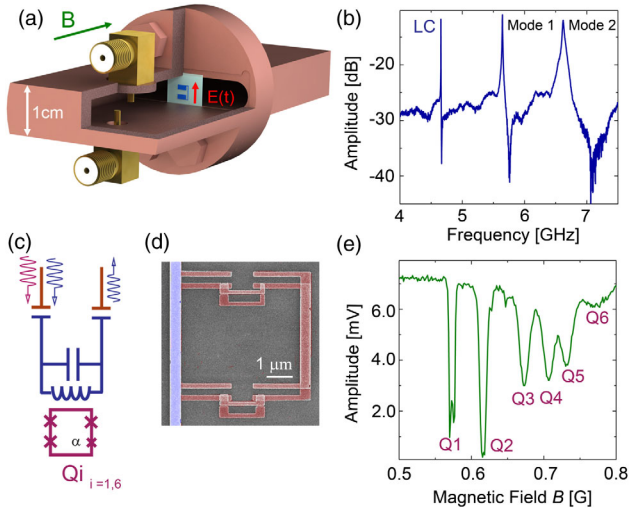

FIG. 1 (color online). (a) Cutaway representation of the 3D cavity, with the LC circuit (in blue) on its sapphire chip. The green arrow represents the applied magnetic field B. The red arrow represents the ac electric field $E(t)$ of the first mode of the cavity. (b) Transmission spectrum of the cavity coupled to the LC resonator. The first peak at frequency $\omega_{LC}/2\pi = 4.643$ GHz corresponds to the resonance of the LC resonator while the two other peaks correspond to the first modes of the cavity. (c)–(d) Circuit diagram and colorized SEM micrograph showing the FQ (in red) inductively coupled to the LC resonator (in blue). (e) Amplitude of the transmitted signal at frequency ω_{LC} as a function of B, showing the signal from the six qubits.

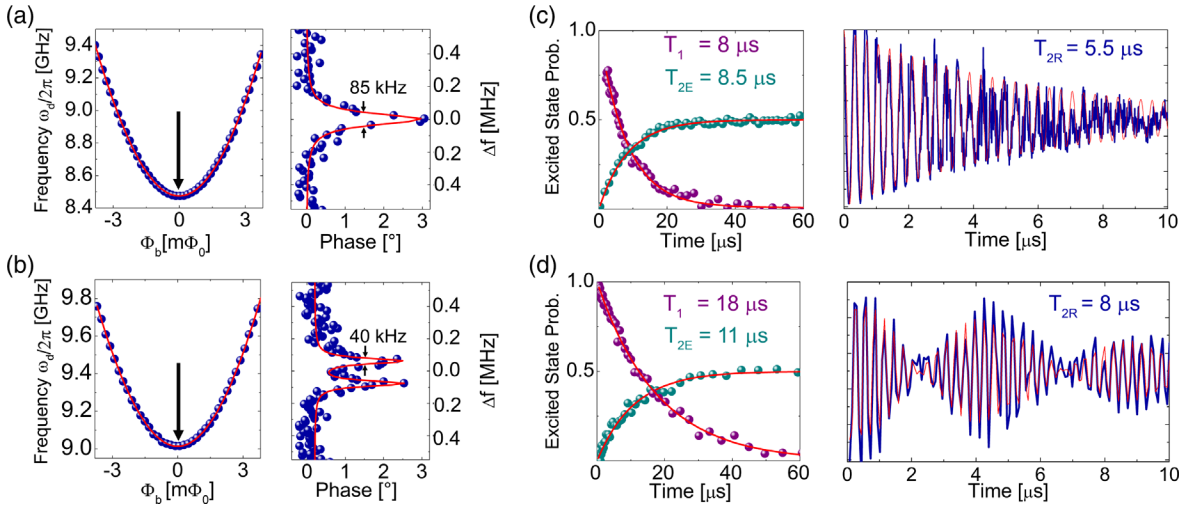

FIG. 2 (color online). Characterization of $Q3$ (top panels) and $Q4$ (bottom panels): (a)–(b) (left panels) Measured qubit frequency $\omega_{01}(\Phi_b)$ (blue dots) and fit (red curve) yielding the qubit parameters Δ and I_P. (Right panels) Spectroscopy data at $\Phi_b = 0$ (blue dots). $Q3$ spectrum is fitted with a single Lorentzian peak; $Q4$ spectrum is fitted with a sum of two Lorentzian peaks separated by 150 kHz. (c)–(d) (left panels) Qubit energy relaxation and spin-echo measurements. The excited state probability is plotted as a function of the delay between the π pulse and readout pulse (blue dots) or between the two $\pi/2$ pulses of the echo sequence (purple dots). Red (orange) solid line is an exponential fit to the energy relaxation (spin-echo) data. (Right panels) Measured Ramsey fringes (blue solid line), with fit (red solid line) to exponentially damped single (top) and double (bottom) sine curves.

resonator acts as an intermediate coupler [15] between the FQs and the first cavity mode. It appears as a resonance peak at $\omega_{LC}/2\pi = 4.643$ GHz in the transmission spectrum [Fig. 1(b)] with a quality factor $Q_{LC} \sim 1.5 \times 10^4$ determined by the length of the input and output antennas inside the cavity [see Fig. 1(a)].

Figure 1(d) presents a colorized SEM micrograph of one of the FQs. It consists of a superconducting aluminum loop of area A intersected by four Josephson junctions. Three of the junctions are identical with a Josephson energy $E_J/h = 250$ GHz and a single electron charging energy $E_C/h = 3.6$ GHz; the fourth junction area is smaller than others by a factor α (see Table I). When the flux threading the loop $\Phi = BA$ is close to half a flux quantum $\Phi_0/2$, the two states characterized by a persistent current $\pm I_P$ in the loop become degenerate, hybridize, and give rise to an energy splitting $\hbar\Delta$ called the flux-qubit gap. This circuit behaves therefore as a two-level system and its transition frequency is $\omega_{01} = \sqrt{\Delta^2 + \varepsilon^2}$ with $\varepsilon = 2I_P\Phi_b/\hbar$ and $\Phi_b = \Phi - \Phi_0/2$ [6,7].

The qubits are fabricated by double angle evaporation of Al–AlOx–Al on sapphire. We use a trilayer PMMA-Ge-MAA process [16,17], which provides a good precision and reproducibility of the junction size and a rigid germanium mask, robust to the O_2 ashing and ion milling cleaning steps, which evacuates efficiently the charges during e-beam lithography. A more precise description of this process is given in [18]. The measurements are performed in a cryogen-free dilution refrigerator at a temperature of 33 mK. The device is magnetically shielded with 2 Cryoperm boxes surrounding a superconducting enclosure. The cavity is also closed using Ecosorb corks and seals, in order to protect the sample from electromagnetic radiation that could generate quasiparticles [27]. The input line is attenuated at low temperature to minimize thermal noise and filtered with impedance-matched radiation-absorbing filters. The readout output line includes several filters, two isolators, and a cryogenic HEMT amplifier. Qubit state manipulations are performed by injecting in the input line microwave pulses at $\omega_d \sim \omega_{01}$, followed by a readout pulse at $\omega_m \sim \omega_{LC}$ whose amplitude and phase yield the qubit excited state probability [28].

An advantage of the cavity readout is the possibility to measure several qubits in a single run, by fabricating them with different loop areas A_i so that the field $B_i = \Phi_0/2A_i$ at which the flux reaches $\Phi_0/2$ is different for each qubit. Figure 1(e) presents the amplitude of the transmitted signal at frequency ω_{LC} as a function of B, showing a dip in the amplitude of the transmitted signal when the frequency of any of the six FQs comes close to ω_{LC}.

Each qubit is characterized by its spectroscopic parameters Δ and I_P, extracted from the dependence of its resonance frequency on the applied flux. These values, given in Table 1, are in good agreement with the predictions of the model described in [18] using both the measured values of α and of the tunnel resistance of the junctions. The coherence properties of each qubit are measured with the appropriate microwave pulse sequence [29]: the energy-relaxation time T_1, the Ramsey coherence time T_{2R} from which one gets the Ramsey pure dephasing time $(T_{\varphi R})^{-1} = (T_{2R})^{-1} - (2T_1)^{-1}$, and the echo decay time T_{2E} yielding the echo pure dephasing time $(T_{\varphi E})^{-1} = (T_{2E})^{-1} - (2T_1)^{-1}$.

We now present detailed measurements on the qubits Q3 and Q4 having the longest coherence times. The flux dependence of their frequency, shown in Figs. 2(a) and 2(b), yields $\Delta/2\pi = 8.47$ (9.01) GHz and $I_P = 169$ (160) nA for $Q3$ ($Q4$). Since both qubits were designed to have the same parameters, this shows good control of our e-beam lithography and oxidation parameters. We now turn to the coherence times at the so-called optimal point $\Phi_b = 0$, where the qubit frequency $\omega_{01} = \Delta$ is insensitive to first order to flux noise [10,11]. Energy relaxation [see Figs. 2(c) and 2(d)] is exponential with $T_1 = 8\ \mu$s for $Q3$ and $18\ \mu$s for $Q4$. Ramsey fringes also show an exponential decay for $Q3$ with $T_{\varphi R} = 8.5\ \mu$s, and an exponentially decaying beating pattern for $Q4$ with $T_{\varphi R} = 10\ \mu$s. These features are consistent with the qubit spectra measured after an excitation pulse of $\sim 20\ \mu$s with a power well below saturation [see Fig. 2(a)]: the $Q3$ line is Lorentzian with a full-width-half-maximum (FWHM) of 85 kHz, while the $Q4$ line consists of a doublet of two Lorentzians separated by 150 kHz and having a width of 40 kHz, whose origin is discussed further below.

The amplitude of the spin-echo signal decays exponentially [see Figs. 2(c) and 2(d)] with finite pure dephasing times $T_{\varphi E} = 17\ \mu$s for $Q3$ and $T_{\varphi E} = 16\ \mu$s for $Q4$. This moderate improvement compared to the Ramsey pure dephasing times points out the presence of high-frequency noise in our circuit in contrast to previous reports [11,13]. We attribute this effect to fluctuations in the photon number (photon noise) of one or several cavity modes inducing fluctuations of the qubit frequency due to the dispersive shift [10,30,31]. This noise cannot be compensated by the echo protocol because its correlation time ($\sim$100 ns–1 μs) given by the mode energy damping is shorter than the echo sequence duration. By plunging the antennas deeper in the cavity for reducing the cavity damping time, the observation of a lower T_{2E} confirms this explanation [30,31]. Interestingly, removing the photon-noise contribution from the Ramsey pure dephasing time yields a "low-frequency Ramsey dephasing time" $(\tilde{T}_{\varphi R})^{-1} = (T_{\varphi R})^{-1} - (T_{\varphi E})^{-1}$ with $\tilde{T}_{\varphi R} = 16\ \mu$s for $Q3$ and $\tilde{T}_{\varphi R} = 30\ \mu$s for $Q4$. This one order of magnitude improvement compared to previous flux-qubit experiments that reported $\tilde{T}_{\varphi R}$ in the 0.2–2.5 μs range at the optimal point [10,11,13] is discussed later.

Away from the optimal point, decoherence is governed mainly by flux noise in agreement with previous works [11,13]. The Ramsey and spin-echo damping become Gaussian as $|\Phi_b|$ increases, which is characteristic of $1/f$ noise [32]. Fitting the Ramsey (or echo) envelope as $f_{R,E}(t) = e^{-t/(2T_1)} e^{-(\Gamma_{\varphi R,E} t)^2}$, we observe a linear dependence of $\Gamma_{\varphi R,E} = (T_{\varphi R,E})^{-1}$ on $|\Phi_b|$, with $\Gamma_{\varphi R} \sim 4.5\ \Gamma_{\varphi E}$ (see Fig. 3), consistent with dephasing caused by flux noise. Indeed, assuming a flux-noise power spectral density $S_\Phi(\omega) = A_\Phi/\omega$, one can show [11,32] that

TABLE I. Parameters of the different measured FQs. Here Δ is the FQ gap, I_P is the persistent current flowing in the loop of the qubit, α corresponds to the measured ratio between the small and big junctions, T_1 is the relaxation time, T_P the Purcell limit time due to the coupling of the qubit with the cavity, $T_{\varphi R}$ and $T_{\varphi E}$ the coherence times at the optimal point obtained by Ramsey and Echo sequences, respectively.

	$\Delta/2\pi$ (GHz)	I_P (nA)	α	T_1 (μs)	T_P (μs)	$T_{\varphi R}$ (μs)	$T_{\varphi E}$ (μs)
$Q1$	2.70	245	0.61	6-10	1.1×10^5	2	7
$Q2$	4.91	207	0.55	2	3	-	-
$Q3$	8.47	169	0.49	6.5–8	30	8	17
$Q4$	9.01	160	0.49	13–18	270	10	16
$Q5$	9.71	171	0.43	5.5–12	90	5	>100
$Q6$	15.15	140	0.4	4	12	-	-

$\Gamma_{\varphi E} = \sqrt{A_\Phi \ln 2}\,|\partial\omega_{01}/\partial\Phi_b|$ and $\Gamma_{\varphi R} = \sqrt{A_\Phi \ln(1/\omega_{\rm IR} t)} \times |\partial\omega_{01}/\partial\Phi_b|$, with $\omega_{\rm IR}$ an infrared cutoff frequency determined by the rate of data acquisition, and $|\partial\omega_{01}/\partial\Phi_b| \simeq 2I_P|\varepsilon|/\hbar\Delta$. In our experiments, $\sqrt{\ln(1/\omega_{\rm IR} t)} \sim 3.7$ predicting $\Gamma_{\varphi R} \sim 4.5\ \Gamma_{\varphi E}$ in agreement with the measured value. We find an amplitude $A_\Phi = (2.5\ \mu\Phi_0)^2$ comparable to previously reported values [11,13].

All six qubits were characterized in this way, over several cooldowns (see Table I). Energy relaxation times were found to change from cooldown to cooldown, and also to occasionally change abruptly in the course of one cooldown. Several mechanisms contribute to relaxation; among them, spontaneous emission of a photon by the qubit in the measurement lines (the so-called Purcell regime [33]). Because this spontaneous emission rate T_P^{-1} is also the rate at which a photon coming from the measurement line is absorbed by the qubit, it can be quantitatively determined by measuring the qubit Rabi frequency Ω_R for a given microwave power $P_{\rm in}$ at the cavity input. For a qubit coupled symmetrically to the input and output lines, one gets

$$T_P = \frac{2}{\Omega_R^2} \frac{P_{\rm in}}{\hbar\omega_{01}}. \quad (1)$$

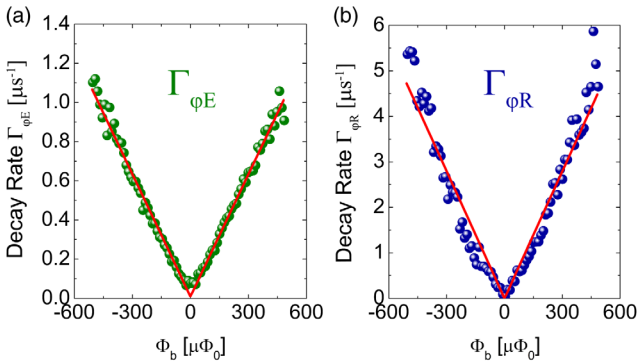

FIG. 3 (color online). Pure dephasing rates of $Q4$ as a function of Φ_b: Experimental (dots) and fitted (line, see text) echo (a) and Ramsey (b) dephasing rates.

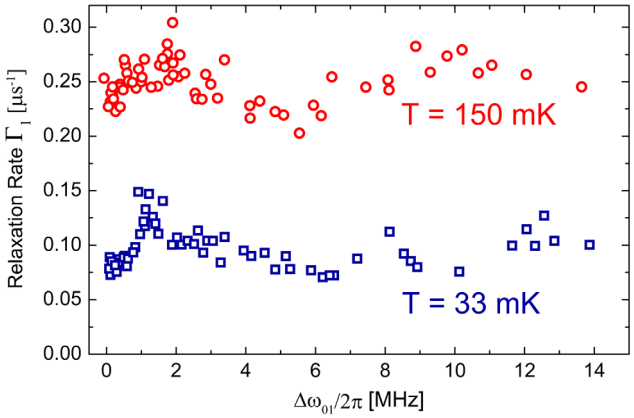

FIG. 4 (color online). Frequency dependence of the relaxation rate Γ_1 of $Q4$ in the vicinity of its optimal point at $T = 33$ mK (blue squares) and $T = 150$ mK (red circles), showing an increased relaxation rate caused by quasiparticles.

Comparing these estimates with the measured T_1 times (see Table I), we find that $Q2$ and $Q6$ are almost Purcell limited. The intrinsic energy relaxation time $1/(T_1^{-1} - T_P^{-1})$ of all six measured qubits at their optimal point is thus in the 6–20 μs range. This significant improvement over previous reports of T_1 in the 0.5–4 μs range [9–11,34] (except one sample for which $T_1 = 12$ μs [13]) is probably due to a combination of several factors: good control of the electromagnetic environment in the 3D cavity [14], careful filtering and shielding against infrared radiation [27], low-loss sapphire substrate, and different fabrication process.

The frequency dependence of the relaxation rate $\Gamma_1 = (T_1)^{-1}$ of $Q4$ in the vicinity of the optimal point is shown in Fig. 4. Large variations are observed, with, in particular, a reproducible increase of the relaxation rate by a factor 2 over 1 MHz, as also recently observed for a transmon qubit [35]. No corresponding anomaly in the Rabi frequency was observed at this point, which excludes spontaneous emission into the measurement lines [see Eq. (1)]. We attribute therefore this peak to one resonant microscopic two-level system (TLS) weakly coupled to the qubit [35]. The remaining constant background $\sim(20\ \mu s)^{-1}$ could be due to dielectric losses, vortex motion, or out-of-equilibrium quasiparticles.

To estimate the quasiparticle contribution to relaxation, the same measurements were performed at 150 mK, a temperature at which the quasiparticle density is expected to be close to its thermal equilibrium value. The relaxation rate increases to $\Gamma_1^{(150\ \mathrm{mK})} \simeq (5\ \mu s)^{-1}$ due to quasiparticles with a similar frequency dependence as at 33 mK, although less pronounced. Assuming that quasiparticles are mainly generated in the pads of the LC resonator and diffuse into the galvanically coupled qubits, we estimate the density of quasiparticles in the vicinity of the qubit $n_{qp}(150\ \mathrm{mK}) = 1\ \mu m^{-3}$ [36]. This density yields a theoretical relaxation rate $\Gamma_1^{(qp)} = (14\ \mu s)^{-1}$ [18], lower than the measured value by a factor 3, a discrepancy which we attribute to the crudeness of the modeling of quasiparticle diffusion. Since $\Gamma_1^{(qp)}$ is proportional to the quasiparticle density [36], we conclude that an out-of-equilibrium quasiparticle density of $\sim 0.3\ \mu m^{-3}$ would be sufficient to explain the measured energy relaxation times at 33 mK, which seems a plausible value in view of earlier reports in other superconducting qubit circuits [14,37,38]. However, the dielectric loss contribution is also important. Taking into account reported values of dielectric loss tangents $\sim 2 \times 10^{-5}$ [18], we find $\Gamma_1^{(\mathrm{dielectric})} \sim (25\ \mu s)^{-1}$, which is comparable to the measured values. Along these lines, we note that flux qubits fabricated on a high resistivity silicon chip and measured with the same setup at 33 mK showed a fivefold increase in relaxation rate.

Another interesting aspect of our experiment is the long Ramsey pure dephasing time $T_{\varphi R}$ measured for $Q3$ and $Q4$ at their flux optimal point. Although not quite as long, all measured qubits have $T_{\varphi R}$ in excess of 3 μs (see Table I). The origin of decoherence at the optimal point for FQs has so far not been identified. One striking feature is the large variability of reported values of $T_{\varphi R}$ at the optimal point for rather similar FQ samples, ranging from 0.2 μs [10] up to 10 μs in this work, whereas $T_{\varphi R} = 2.5$ μs in [13]. A doublet structure in the qubit line was frequently observed at the optimal point [10,11,39], with a greatly varying splitting [20 MHz in [10] and 150 kHz in this work, as seen in Fig. 2(b)], which was also found to vary in time.

All these features are consistent with charge noise being the dominant noise source limiting $T_{\varphi R}$ at the optimal point. The sensitivity to this noise is exponentially dependent on the ratio E_J/E_C [7], which is twice smaller in [10] compared to the present work. Using the model described in [18], we estimate a charge modulation amplitude of $\sim$50 kHz for $Q3/Q4$ compared to $\sim$120 MHz for [10] ($\sim$300 kHz for [13]), yielding a 3 orders of magnitude lower charge noise sensitivity which explains qualitatively the difference in dephasing time. The doublet line shape of $Q4$ can be attributed to slow fluctuations of the electron number parity on one of the qubit islands [39], as observed for transmon qubits [38,40].

In conclusion, we have characterized the coherence properties of six FQs in a three-dimensional microwave cavity. We consistently find intrinsic energy relaxation times T_1 ranging between 6 and 20 μs, a significant improvement over previous FQ measurements that we attribute to good control of the electromagnetic environment provided by the 3D cavity, low-loss substrate, and careful filtering. We identify weakly coupled two-level systems, quasiparticles, and dielectric losses as likely sources of energy damping. At the optimal point, long Ramsey pure dephasing times up to 10 μs are measured, limited by a combination of photon noise and charge noise with roughly equal contribution. We argue that charge noise is the dominant microscopic dephasing mechanism for FQs at the optimal point, and that its effect can be greatly mitigated

by choosing proper qubit parameters. Our results prove that FQs can reliably reach long coherence times, which opens new perspectives for the field of hybrid quantum circuits, in particular, for the coherent coupling of single spins to superconducting circuits.

We would like to acknowledge fruitful discussions with M. Devoret, A. Lupascu and within the Quantronics group. We thank P. Sénat, P.-F. Orfila, D. Duet, J.-C. Tack, P. Pari, D. Bouville, P. Forget, and M. de Combarieu for their technical support. This work was supported by the ANR CHIST-ERA project QINVC, the C'Nano IdF project QUANTROCRYO, the ERC project CIRQUSS, the JSPS, and by the EU under REA Grant Agreement No. CIG-618258 (G. C.).

*michael.stern@cea.fr

[1] N. Bar-Gill, L. M. Pham, A. Jarmola, D. Budker, and R. L. Walsworth, Nat. Commun. **4**, 1743 (2013).
[2] A. Morello *et al.*, Nature (London) **467**, 687 (2010).
[3] K. Saeedi, S. Simmons, J. Z. Salvail, P. Dluhy, H. Riemann, N. V. Abrosimov, P. Becker, H.-J. Pohl, J. J. L. Morton, and M. L. W. Thewalt, Science **342**, 830 (2013).
[4] D. Marcos, M. Wubs, J. M. Taylor, R. Aguado, M. D. Lukin, and A. S. Sørensen, Phys. Rev. Lett. **105**, 210501 (2010).
[5] J. Twamley and S. D. Barrett, Phys. Rev. B **81**, 241202 (2010).
[6] J. E. Mooij *et al.*, Science **285**, 1036 (1999).
[7] T. Orlando, J. Mooij, L. Tian, C. van der Wal, L. Levitov, S. Lloyd, and J. Mazo, Phys. Rev. B **60**, 15 398 (1999).
[8] C. H. van der Wal *et al.*, Science **290**, 773 (2000).
[9] I. Chiorescu, Y. Nakamura, C. J. P. M. Harmans, and J. E. Mooij, Science **299**, 1869 (2003).
[10] P. Bertet, I. Chiorescu, G. Burkard, K. Semba, C. Harmans, D. DiVincenzo, and J. Mooij, Phys. Rev. Lett. **95**, 257002 (2005).
[11] F. Yoshihara, K. Harrabi, A. O. Niskanen, Y. Nakamura, and J. S. Tsai, Phys. Rev. Lett. **97**, 167001 (2006).
[12] P. Forn-Díaz, J. Lisenfeld, D. Marcos, J. J. García-Ripoll, E. Solano, C. J. P. M. Harmans, and J. E. Mooij, Phys. Rev. Lett. **105**, 237001 (2010).
[13] J. Bylander, S. Gustavsson, F. Yan, F. Yoshihara, K. Harrabi, G. Fitch, D. G. Cory, Y. Nakamura, J.-S. Tsai, and W. D. Oliver, Nat. Phys. **7**, 565 (2011).
[14] H. Paik *et al.*, Phys. Rev. Lett. **107**, 240501 (2011).
[15] I. M. Pop, K. Geerlings, G. Catelani, R. J. Schoelkopf, L. I. Glazman, and M. H. Devoret, Nature (London) **508**, 369 (2014).
[16] J. Romijn and E. van der Drift, Physica (Amsterdam) **152B**, 14 (1988).
[17] H. Pothier, Ph.D thesis, SPEC-CEA Saclay (1991).
[18] See Supplemental Material at http://link.aps.org/supplemental/10.1103/PhysRevLett.113.123601 for a detailed description of the fabrication process of the flux qubits, the model of a 4-junction flux qubit including the geometric capacitance terms and the relaxation rate calculations due to quasiparticles and dielectric losses, which includes Refs. [19–26].
[19] CST EM Studio, Computer Simulation Technology, https://www.cst.com/Products/CSTEMS.
[20] G. Catelani, M. Stern, and P. Bertet (to be published).
[21] J. Aumentado, M. W. Keller, J. M. Martinis, and M. H. Devoret, Phys. Rev. Lett. **92**, 066802 (2004).
[22] L. J. Geerligs, M. Peters, L. E. M. deGroot, A. Verbruggen, and J. E. Mooij, Phys. Rev. Lett. **63**, 326 (1989).
[23] V. Bouchiat, Ph.D thesis, SPEC-CEA Saclay, 1998.
[24] L. Bretheau, Ph.D thesis, SPEC-CEA Saclay, 2013.
[25] G. Catelani, J. Koch, L. Frunzio, R. J. Schoelkopf, M. H. Devoret, and L. I. Glazman, Phys. Rev. Lett. **106**, 077002 (2011).
[26] A. D. O'Connell *et al.*, Appl. Phys. Lett. **92**, 112903 (2008).
[27] R. Barends *et al.*, Appl. Phys. Lett. **99**, 113507 (2011).
[28] A. Blais, R. S. Huang, A. Wallraff, S. M. Girvin, and R. J. Schoelkopf, Phys. Rev. A **69**, 062320 (2004).
[29] D. Vion *et al.*, Science **296**, 886 (2002).
[30] C. Rigetti *et al.*, Phys. Rev. B **86**, 100506 (2012).
[31] A. P. Sears, A. Petrenko, G. Catelani, L. Sun, H. Paik, G. Kirchmair, L. Frunzio, L. I. Glazman, S. M. Girvin, and R. J. Schoelkopf, Phys. Rev. B **86**, 180504(R) (2012).
[32] G. Ithier *et al.*, Phys. Rev. B **72**, 134519 (2005).
[33] A. A. Houck *et al.*, Phys. Rev. Lett. **101**, 080502 (2008).
[34] J. E. Johnson, C. Macklin, D. H. Slichter, R. Vijay, E. B. Weingarten, J. Clarke, and I. Siddiqi, Phys. Rev. Lett. **109**, 050506 (2012).
[35] R. Barends *et al.*, Phys. Rev. Lett. **111**, 080502 (2013).
[36] G. Catelani, R. J. Schoelkopf, M. H. Devoret, and L. I. Glazman, Phys. Rev. B **84**, 064517 (2011).
[37] P. J. de Visser, J. J. A. Baselmans, P. Diener, S. J. C. Yates, A. Endo, and T. M. Klapwijk, Phys. Rev. Lett. **106**, 167004 (2011).
[38] D. Ristè, C. C. Bultink, M. J. Tiggelman, R. N. Schouten, K. W. Lehnert, and L. DiCarlo, Nat. Commun. **4**, 1913 (2013).
[39] M. Bal, M. H. Ansari, J.-L. Orgiazzi, R. M. Lutchyn and A. Lupascu, arXiv:1406.7350.
[40] J. A. Schreier *et al.*, Phys. Rev. B, **77**, 180502 (2008).